Baryonic Effects on Lagrangian Clustering and Angular Momentum Reconstruction

Sheng, MJ

2023-02-01

CrossMark

Baryonic Effects on Lagrangian Clustering and Angular Momentum Reconstruction

Ming-Jie Sheng[1] , Hao-Ran Yu[1] , Sijia Li[1] , Shihong Liao[2,3] , Min Du[1] , Yunchong Wang[4,5] , Peng Wang[6] ,
Kun Xu[7] , Shy Genel[8,9] , and Dimitrios Irodotou[2]

[1] Department of Astronomy, Xiamen University, Xiamen, Fujian 361005, People's Republic of China; haoran@xmu.edu.cn
[2] Department of Physics, University of Helsinki, Gustaf Hällströmin katu 2, FI-00014 Helsinki, Finland
[3] Key Laboratory for Computational Astrophysics, National Astronomical Observatories, Chinese Academy of Sciences, Beijing 100101, People's Republic of China
[4] Department of Physics, Stanford University, 382 Via Pueblo Mall, Stanford, CA 94305, USA
[5] Kavli Institute for Particle Astrophysics and Cosmology, P.O. Box 2450, Stanford University, Stanford, CA 94305, USA
[6] Shanghai Astronomical Observatory, 80 Nandan Road, Shanghai 200030, People's Republic of China
[7] Department of Astronomy, School of Physics and Astronomy, Shanghai Jiao Tong University, Shanghai 200240, People's Republic of China
[8] Center for Computational Astrophysics, Flatiron Institute, 162 Fifth Avenue, New York, NY 10010, USA
[9] Columbia Astrophysics Laboratory, Columbia University, 550 West 120th Street, New York, NY 10027, USA

Abstract

Recent studies illustrate the correlation between the angular momenta of cosmic structures and their Lagrangian properties. However, only baryons are observable and it is unclear whether they reliably trace the cosmic angular momenta. We study the Lagrangian mass distribution, spin correlation, and predictability of dark matter, gas, and stellar components of galaxy–halo systems using IllustrisTNG, and show that the primordial segregations between components are typically small. Their protoshapes are also similar in terms of the statistics of moment of inertia tensors. Under the common gravitational potential they are expected to exert the same tidal torque and the strong spin correlations are not destroyed by the nonlinear evolution and complicated baryonic effects, as confirmed by the high-resolution hydrodynamic simulations. We further show that their late-time angular momenta traced by total gas, stars, or the central galaxies, can be reliably reconstructed by the initial perturbations. These results suggest that baryonic angular momenta can potentially be used in reconstructing the parameters and models related to the initial perturbations.

1. Introduction

The large-scale structure (LSS) of the universe is primarily driven by the dynamics of dark matter (DM). After recombination, baryonic matter decouples from radiation and follows the clustering of DM under gravity. Hence, the matter distribution on a large scale can be probed by various tracers, such as galaxies, resulting in rich cosmological information (e.g., Peebles 1969; Rimes & Hamilton 2005; McQuinn 2021). At low redshifts, the nonlinear structure formation generates vorticities in the matter velocity field. This nondecaying small-scale vector mode actually reflects primordial density perturbation on larger scales, via the tidal torque theory (Doroshkevich 1970; White 1984). In particular, the tidal environments of the protohalos in the Lagrangian space, characterized by the Hessian of the primordial gravitational potential, torque those protohalos in a persistent way such that the virialized DM halos at low redshifts tend to keep the predicted angular momentum directions (Porciani et al. 2002) and magnitudes (Wu et al. 2021). Thus, their angular momenta provide independent cosmological information, including, e.g., the reconstruction of primordial density and tidal fields (Lee & Pen 2000, 2001), the effects of cosmic neutrino mass (Yu et al. 2019; Lee et al. 2020) and dark energy (Lee & Libeskind 2020), possible detection of chiral violation (Yu et al. 2020; Motloch et al. 2022), and the understanding of galaxy intrinsic

alignments (e.g., Catelan et al. 2001; Blazek et al. 2011; Schmidt et al. 2015; Wang & Kang 2018).

Unfortunately, unlike the mass of DM halos that can be inferred by gravitational lensing, the rotation of DM halos are difficult to observe, and one can only expect the angular momenta of galaxies or other baryonic tracers to be the proxies of that of DM halos. The three-dimensional (3D) spins (hereafter we refer to "angular momentum direction" as "spin" for brevity) of galaxies are readily observable (see the discussions in Iye et al. 2019; Motloch et al. 2021). This parity-odd observable is free from the contamination of linear perturbation theory, and many approaches are trying to understand it observationally or theoretically. Most recently, Yu et al. (2020) proposed the idea of predicting the spin mode of protohalos by using the E-mode clustering in Lagrangian space, referred to as "spin reconstruction," and by using this method Motloch et al. (2021) for the first time discover a weak but significant correlation between the observational galaxy spins and the reconstructed cosmic initial conditions.

The importance of this correlation deserve further explanation and investigation. First, the reconstructed initial conditions, given by ELUCID (Wang et al. 2014, 2016), use only galaxy positions without their spins, so the correlation demonstrates that the spins of cosmic structures, even traced by baryons, indeed contain additional cosmological information beside galaxy/halo locations. Second, the correlation is found in Lagrangian space, where Fourier modes are still linear and directly related to cosmological constraints. Third, this observational attempt involves both known and unknown physical processes and systematic errors. Regarding the last point, the errors include those in the reconstructed initial

Table 1
Counts of Halos and Mean Galaxy Counts per Halo (Galaxies with Stellar Mass Threshold $M_s = 10^9 \, h^{-1} \, M_\odot$) in Different Mass Bins (Mass Units: $h^{-1} \, M_\odot$)

Halo Mass	Halo Counts	Mean Galaxy Counts per Halo
$[10^{11.5}, 10^{12})$	2956	1.2
$[10^{12}, 10^{12.5})$	1051	2.1
$[10^{12.5}, 10^{13})$	355	4.9
$[10^{13}, 10^{13.5})$	124	13.2
$[10^{13.5}, +\infty)$	60	63.6

conditions, in the Lagrangian space remapping (S. Li et al. 2022, in preparation), and in the complicated observations of galaxy spins, etc. While these techniques continue to be improved, the underlying gravitational and baryonic processes are yet to be studied separately. In particular, it is still unclear whether and how baryonic components trace the DM across the cosmic evolution and galaxy formation. The baryonic effects include gas cooling, star and galaxy formation, and supernova and black hole feedbacks, which are highly nonlinear and their effects on baryonic angular momenta cannot be modeled by cosmological perturbation theories. In this work, we use the state-of-the-art magnetohydrodynamic (MHD) simulations IllustrisTNG (Marinacci et al. 2018; Nelson et al. 2018, 2019a, 2019b; Pillepich et al. 2018, 2019; Springel et al. 2018) to study these baryonic effects on the angular momentum generation, and quantify how these primordial spin modes can be traced by the baryonic matter at low redshifts.

In the rest of this article, Section 2 describes the simulation and basic analyses. Section 3 shows the spin conservation and reconstruction results for DM and baryonic components. The conclusion and discussion are presented in Section 4.

2. Methodology and Basic Analyses

The IllustrisTNG simulations are a suite of MHD galaxy formation simulations using the AREPO code (Springel 2010; Weinberger et al. 2020). In this study, the main results are given by the TNG100-1 simulation, which starts with 1820^3 DM particles and 1820^3 gas cells in a periodic cubic box with a comoving length $75 \, h^{-1}$ Mpc per side. The initial condition is generated with the N-GENIC code (Springel et al. 2005) by perturbing a "glass" particle load (White 1996) with the Zel'dovich approximation. The adopted cosmological parameters are from the Plank 2015 results (Planck Collaboration et al. 2016), i.e., $\Omega_m = 0.3089$, $\Omega_b = 0.0486$, $\Omega_\Lambda = 0.6911$, and $h = 0.6774$. The mass resolutions for DM particles and gas cells are $m_{DM} = 5.1 \times 10^6 \, h^{-1} M_\odot$ and $m_{gas} = 9.4 \times 10^5 \, h^{-1} M_\odot$ (on average), respectively.

DM halos and subhalos are identified with friends-of-friends (FOF; Davis et al. 1985) and SUBFIND algorithms (Springel et al. 2001). The halo total mass M_{tot} is defined as the sum of the individual mass of every particle/cell, of all types in consideration, i.e., DM, gas, and stars. We only consider FOF halos with total mass $M_{tot} \geqslant 10^{11.5} \, h^{-1} M_\odot$, yielding a halo catalog contains 4546 samples with particle IDs, positions, velocities, and other astrophysical properties for DM, gas, and stellar components. Shown in Table 1, the total samples are divided into five mass bins and list halo counts in each mass bin.

To study the primordial spin mode, we need to trace the halo mass elements back to Lagrangian space. For DM, we can simply trace them by following the particle IDs. For gas cells

and star particles, we trace their tracer particles (Genel et al. 2013) back to the initial condition. The TNG100-1 simulation contains 2×1820^3 tracer particles. To see the distribution of each component of halos and corresponding protohalos more intuitively, in Figure 1, we randomly select four halos in four different mass bins of Table 1 and plot the column density projected onto the x–y plane. Subpanels correspond to different components in Lagrangian (initial condition) and Eulerian (redshift $z = 0$) spaces, respectively. The halo masses, halo IDs, and coordinates in TNG100-1 are explicitly shown in the figure.

The mass distributions in Lagrangian space play important roles in the angular momentum production, in which the Lagrangian space volume occupation (size), center-of-mass (CoM) location, and 3D shape are key ingredients. The Lagrangian size is directly related to the total halo mass; the CoM location can be reliably reconstructed (S. Li et al. 2022, in preparation); and the 3D shape can be characterized, up to the second moment (quadrupole), by the moment of inertia tensor. Since the structure formation inside each DM halo is mostly virialized, we expect, and it is verified by simulation that, the above properties for different components are similar.

Focusing on the sizes first, despite the mass distributions of DM and gas are quite diffuse in Eulerian space while on the contrary for stars, their Lagrangian sizes are all comparable to the equivalent protohalo radius r_q, indicated by radii of circles in Figure 1. Here r_q is defined as

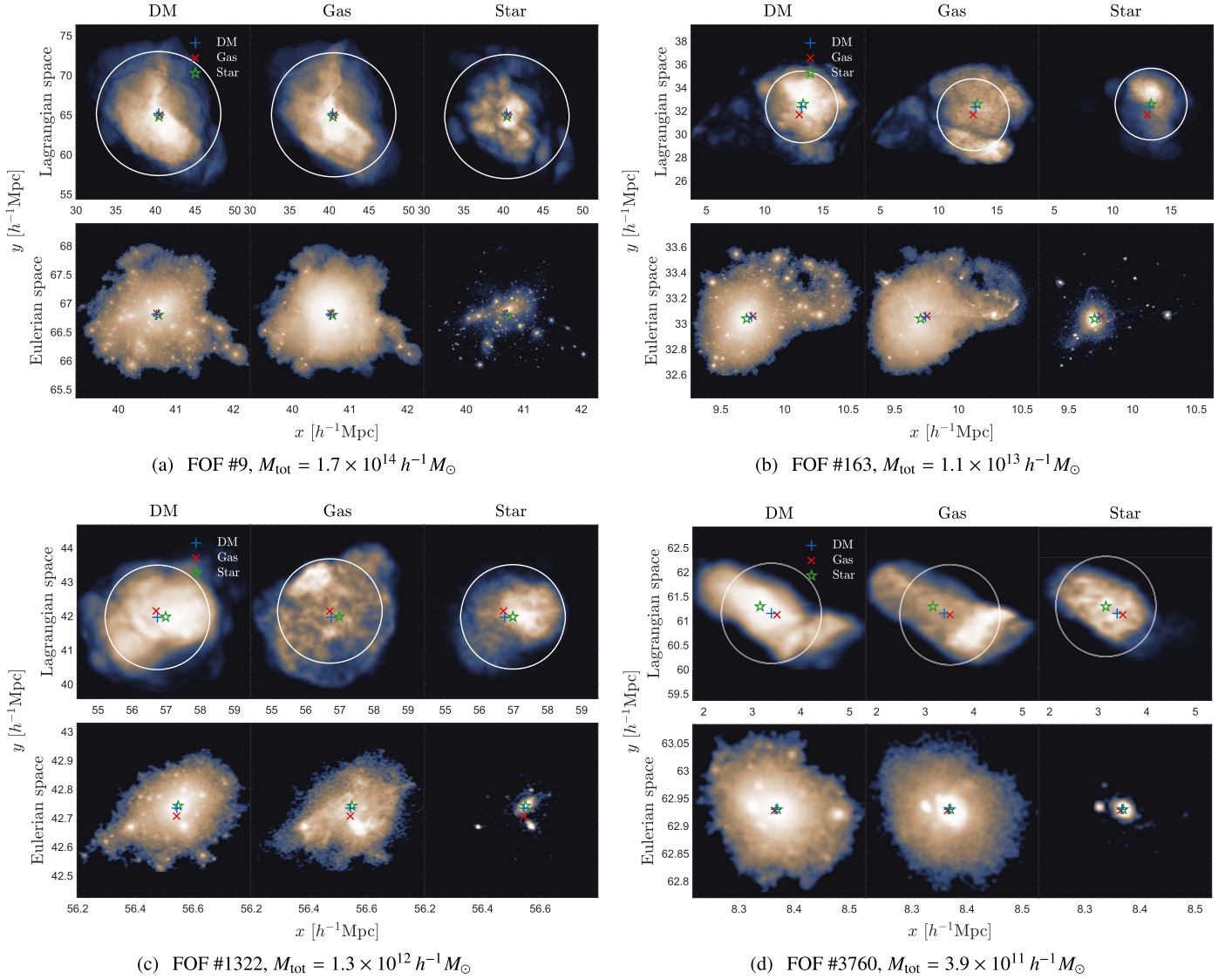$$r_q \equiv \left(\frac{2 M_{tot} G}{\Omega_m H_0^2} \right)^{1/3}, \tag{1}$$

where G is the Newton's constant and H_0 is the Hubble's constant.

Next, we quantify CoM offsets. In Lagrangian and Eulerian spaces, the $+, \times, \star$ symbols represent CoM positions of DM, gas, and stellar components respectively. Due to the baryonic effects, the Lagrangian–Eulerian mappings of DM and baryons are not exactly the same (Liao et al. 2017) and result in these CoM offsets. The top left panel of Figure 2 shows the distribution of CoM offsets Δq normalized by r_q, for each halo mass bin. The Lagrangian CoM offsets of different components are typically small compared to their physical sizes. Especially, for more-massive halos, both the offset and the deviation become smaller. This mass dependence could be explained by the fact that a deeper gravitational potential is more capable of locking baryons, and thus the system is less affected by the environment, and consequently different components are more likely to originate from the same Lagrangian region.

The moment of inertia tensor $I_{jk} = \sum_i m_i x'_j x'_k$ describes the shape of a mass distribution up to quadrupole, where m_i is the particle mass, and x' is the particle position relative to CoM. The eigen-decomposition of I_{jk} gives the the primary, intermediate, and minor axes of the mass distribution and their spatial alignments. The eigenvalues are sorted as $\lambda_1 > \lambda_2 > \lambda_3$, associated with the eigenvectors V_1, V_2, V_3. We use 3D ellipticity

$$e = \frac{\lambda_1 - \lambda_3}{2(\lambda_1 + \lambda_2 + \lambda_3)}, \tag{2}$$

and the alignment eigenvectors to characterize the shape and alignment correlations. For the latter, the alignments are quantified by the cosine μ_i ($i = 1, 2, 3$) of the acute angle

(a) FOF #9, $M_{\text{tot}} = 1.7 \times 10^{14} \, h^{-1} M_{\odot}$

(b) FOF #163, $M_{\text{tot}} = 1.1 \times 10^{13} \, h^{-1} M_{\odot}$

(c) FOF #1322, $M_{\text{tot}} = 1.3 \times 10^{12} \, h^{-1} M_{\odot}$

(d) FOF #3760, $M_{\text{tot}} = 3.9 \times 10^{11} \, h^{-1} M_{\odot}$

Figure 1. Projected column density of DM, gas, and stellar components in Lagrangian and Eulerian spaces. Their CoM are marked by respective symbols. The radii of circles in Lagrangian space indicate r_q.

between V_i of the components in comparison. In the top right panel and bottom panels of Figure 2, we plot the correlation of ellipticity between different components, with overall axes alignment offsets $\sum_{i=1}^{3}(1 - \mu_i)$ indicated by colors. We can see that, for each halo–galaxy system, the Lagrangian counterparts for three components generally have similar shapes and spatial alignments. The Pearson correlation coefficients $r(e_{\text{DM}}, e_{\text{gas}})$, $r(e_{\text{DM}}, e_{\text{star}})$, $r(e_{\text{gas}}, e_{\text{star}})$ are shown in the three subpanels.

3. Results

3.1. Alignment and Conservation of Spins

In this section we start with a study on the spin properties of DM and baryons of halos. In Lagrangian (Eulerian) space, the angular momentum vector $\boldsymbol{j}_L$ ($\boldsymbol{j}_E$) of a certain component (e.g., DM, gas, or stars) is computed as

$$\boldsymbol{j}_L = \sum_i m_i (\boldsymbol{q}_i - \bar{\boldsymbol{q}}) \times (\boldsymbol{u}_i - \bar{\boldsymbol{u}}), \qquad (3)$$

$$\boldsymbol{j}_E = \sum_i m_i (\boldsymbol{x}_i - \bar{\boldsymbol{x}}) \times (\boldsymbol{v}_i - \bar{\boldsymbol{v}}), \qquad (4)$$

where m_i, $\boldsymbol{q}_i$ ($\boldsymbol{x}_i$) and $\boldsymbol{u}_i$ ($\boldsymbol{v}_i$) are the particle mass, Lagrangian (Eulerian) position, and velocity of the ith particle, while $\bar{\boldsymbol{q}}$ ($\bar{\boldsymbol{x}}$) and $\bar{\boldsymbol{u}}$ ($\bar{\boldsymbol{v}}$) are the Lagrangian (Eulerian) CoM position and mean velocity of this component.

We use the cosine of the angle between two vectors $\boldsymbol{j}_L$ and $\boldsymbol{j}_E$ to quantify the cross-correlation between their directions,

$$\mu(\boldsymbol{j}_L, \boldsymbol{j}_E) \equiv \frac{\boldsymbol{j}_L \cdot \boldsymbol{j}_E}{|\boldsymbol{j}_L| \, |\boldsymbol{j}_E|} \in [-1, 1]. \qquad (5)$$

Randomly distributed 3D vectors results in a top-hat distribution of μ with $\langle \mu \rangle = 0$. The top left panel of Figure 3 shows the probability density functions (PDFs) of $\mu(\boldsymbol{j}_L, \boldsymbol{j}_E)$ for DM, gas, and stellar components of all samples. The expectation values $\langle \mu \rangle$ take 0.68, 0.64, and 0.60, respectively, and the PDFs of $\mu(\boldsymbol{j}_L, \boldsymbol{j}_E)$ obviously depart from a top-hat distribution, suggesting that $\boldsymbol{j}_L, \boldsymbol{j}_E$ directions for each component are strongly correlated. Note that comparing to the DM component, the gas and stellar
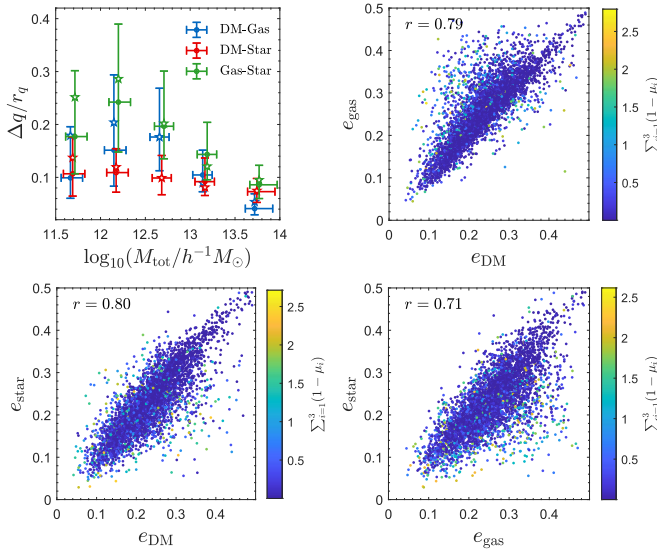
Figure 2. Quantification of the mass distributions of DM, gas, and stellar components in Lagrangian space. The top left panel shows the distributions of normalized CoM offsets $\Delta q/r_q$ for five halo mass bins. The center, lower/upper boundaries of the error bar represent the median, 25%/75% quartiles of the distribution. Note that the distribution is not Gaussian and thus not symmetric; "⋆" symbols indicate the expectation values of the distributions. The remaining three panels show the alignments of Lagrangian distributions. We use ellipticity to characterize the shape. Points are colored according to the overall axes alignment offsets $\sum_{i=1}^{3}(1-\mu_i)$.

components have experienced a series of baryonic processes (e.g., DeFelippis et al. 2017), especially the stellar and AGN feedback (e.g., Zjupa & Springel 2017), but they still remain a strong correlation. This indicates that the memory of the initial tidal fields of the baryonic components is not fully erased by the baryonic processes. In addition, the stellar component shows a weaker correlation compared to gas, which could be explained by the fact that the galaxy stellar spins are affected by galaxy merger events (e.g., Lee & Moon 2022) and star formation processes. In the middle left and bottom left panels of Figure 3, we show the correlations of spins between different components in Lagrangian and Eulerian spaces, respectively. The middle left panel suggests that the spins for each component of protohalos are strongly correlated, which originates from the similar mass distributions of these components and the same tidal torque they feel in Lagrangian space, as shown in Figure 2. In addition, the gas and stellar components show weaker correlations, which is consistent with the result of Figure 2 that these two components show a larger Lagrangian CoM offset and weaker similarity in shape. The bottom left panel shows that these alignments are well conserved through the cosmic evolution. Considering the halo mass dependence of these correlations, the right panels in Figure 3 show that, more-massive halos have a better conservation of spins for each component through the cosmic evolution, and they also show a stronger alignment of spins between different components.

3.2. Spin Reconstruction

In this section we reconstruct the spins for baryonic components based on their Lagrangian space properties analogous to the spin reconstruction of DM component. In the tidal torque theory, the initial angular momentum vector of
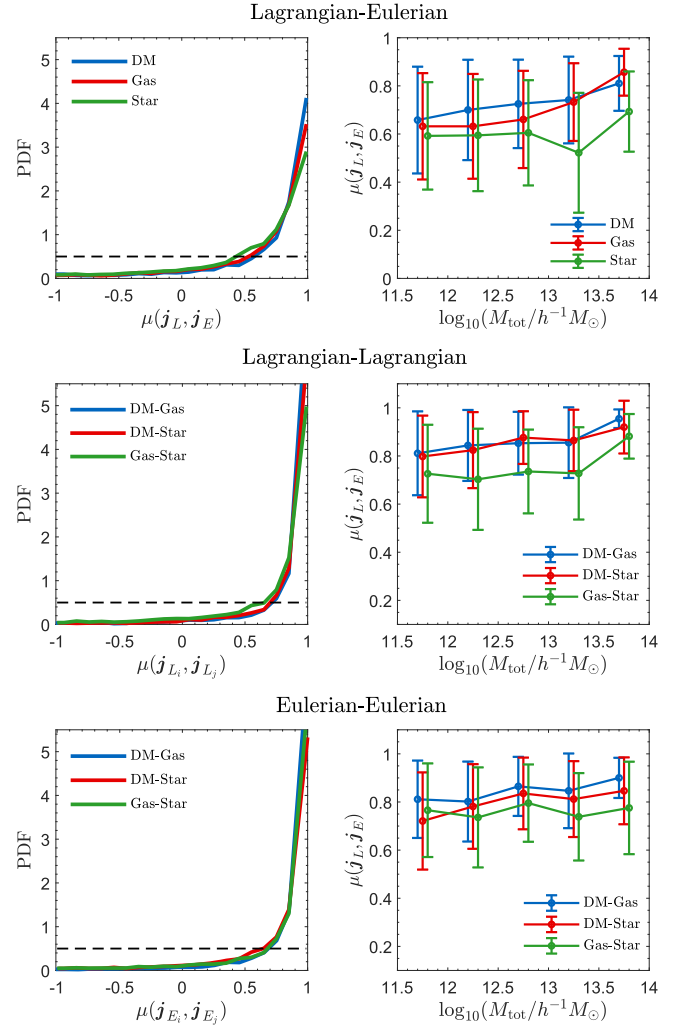
Figure 3. Conservation of spins of DM, gas and stellar components through the cosmic evolution (top) and alignment of spins between these components in Lagrangian (middle) and Eulerian (bottom) spaces. The left panels show the PDFs of $\mu(\boldsymbol{j}_L, \boldsymbol{j}_E)$, $\mu(\boldsymbol{j}_{L_i}, \boldsymbol{j}_{L_j})$ and $\mu(\boldsymbol{j}_{E_i}, \boldsymbol{j}_{E_j})$, where $i, j =$ DM, gas, and stellar components in colored solid lines, with black dotted line indicates the PDF of a random distribution. The right panels show the average μ as a function of halo total mass binned following Table 1. Error bars represent the standard deviation of the distributions.

a protohalo that initially occupies Lagrangian volume V_L is approximately by

$$j_\alpha \propto \epsilon_{\alpha\beta\gamma} I_{\beta\kappa} T_{\kappa\gamma}, \quad (6)$$

where $\boldsymbol{I} = (I_{\beta\kappa})$ is the moment of inertia tensor of V_L, $\boldsymbol{T} = (T_{\kappa\gamma})$ is the tidal tensor acting on $\boldsymbol{I}$, and $\epsilon_{\alpha\beta\gamma}$ is the 3D Levi-Civita symbol. Yu et al. (2020) propose the spin-reconstruction method for halo spins as

$$\boldsymbol{j}_R = (j_\alpha)_R \propto \epsilon_{\alpha\beta\gamma} \mathcal{T}_{\beta\kappa} \mathcal{T}_{\kappa\gamma}^+, \quad (7)$$

where $\mathcal{T}_{\beta\kappa}$ and $\mathcal{T}_{\kappa\gamma}^+$ are tidal fields constructed as the Hessian of the initial gravitational potential smoothed at two different scales r, R.

We use the N-GENIC code to obtain the gravitational potential field ϕ of the TNG100-1 initial condition, and convolve ϕ with a Gaussian window function to obtain the smoothed potential field for calculating $\mathcal{T}_{\beta\kappa}$ and $\mathcal{T}_{\kappa\gamma}^+$. The actual calculation is done in Fourier space (Yu et al. 2020).
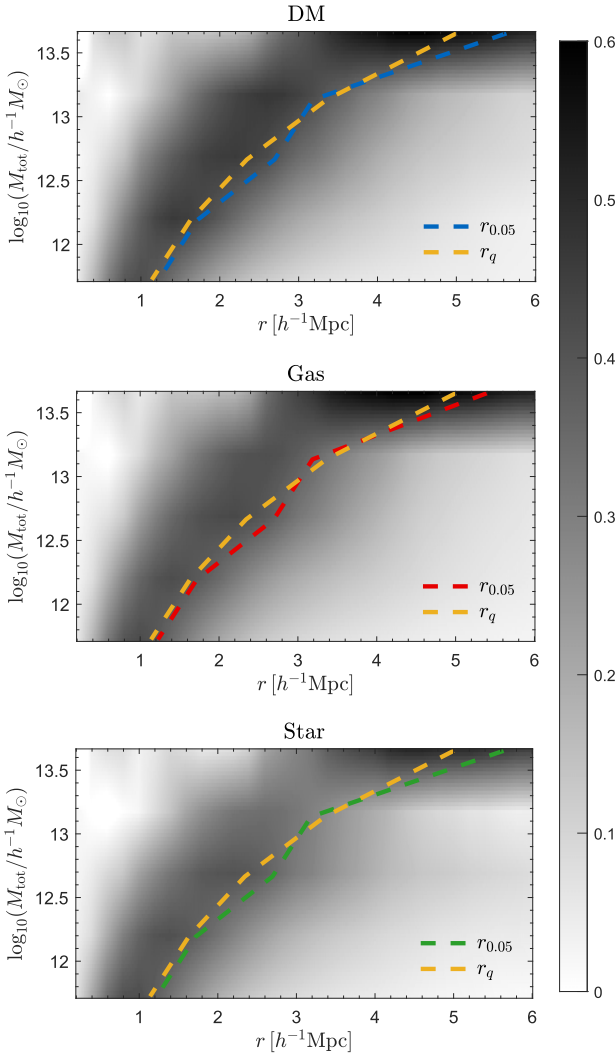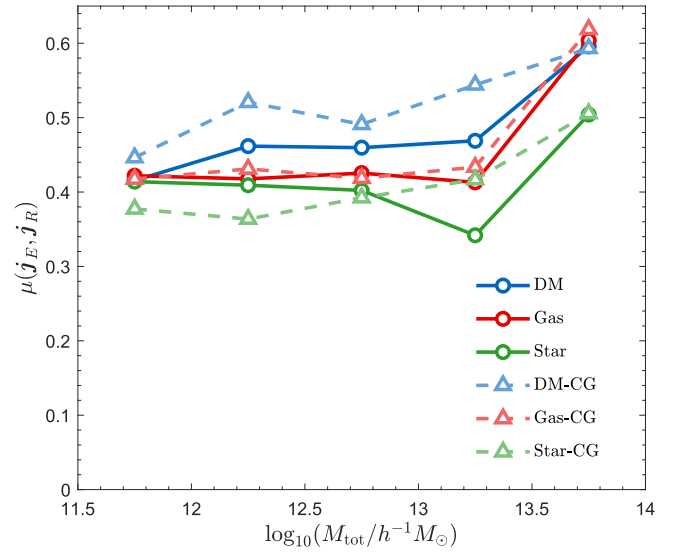
Figure 4. The cross-correlation coefficients between Eulerian j_E halo spins and spins reconstructed using Equation (7) from known initial conditions j_R for DM, gas, and stellar components. Darker colors show better reconstruction. Optimal $r_{0.05}$ (blue, red, and green dashed curves) and the Lagrangian equivalent radius r_q (yellow dashed curves) of the protohalo are also plotted.

Here we characterize the smoothing scale of the Gaussian window function by defining the radius $r_{0.05}$ at which the window function drops to 5% of its maximum.

We cross-correlate the spins j_E of each halo component in Eulerian space with the spins j_R reconstructed by applying Equation (7). We follow Yu et al. (2020), which suggests that by choosing $R \rightarrow r_+$ the cross-correlation maximizes. In Figure 4, from top to bottom, we plot the cross-correlation coefficients $\mu(j_E, j_R)$ for DM, gas, and stellar components and the optimal $r_{0.05}$ which maximize μ in different mass bins. We find that, for different components, the optimal $r_{0.05}$ are fairly similar and close to the equivalent protohalo radius r_q in Lagrangian space.

In Figure 5, we plot the maximally achievable cross-correlation coefficients as a function of halo total mass for DM, gas, and stellar components of total halos. The DM component has a maximum cross-correlation between 0.4 and 0.6, while slightly lower for gas and stellar components. This discrepancy is similar to Figure 3 in that the gas and stellar components have experienced a series of baryonic processes. But overall they still have a maximally achievable cross-correlation of 0.35

Figure 5. Maximally achievable cross-correlation coefficients as a function of halo total mass for components of total halos (solid line) and central galaxies (dashed line). The results for DM, gas, and stellar components are plotted in blue, red, and green, respectively.

to 0.5, which opens up the possibility of using the spins of gas and stellar components to constrain the cosmic initial conditions.

The DM halos in the sample could contain more than one galaxy, shown in Table 1. They include one central galaxy and possibly several satellite galaxies. The angular momentum of such a galaxy–halo system includes individual galaxy spin angular momenta $\sum j_{spin}$ and orbit angular momentum j_{orb}. We further compute the cross-correlation between the spin angular momenta of the central galaxy $j_{spin,CG}$ of each halo and the reconstructed halo spins. In Figure 5, by repeating the similar analyses for the components of total halo, we obtain a similar statistical correlation for central galaxies.

4. Conclusion and Discussion

We study the conservation and predictability of the spins of DM, gas, and stellar components of galaxy–halo systems in TNG100-1 simulation. We conclude the following:

1. The mass distributions of the DM, gas, and stellar components of galaxy–halo systems in Lagrangian space are quite similar, in terms of locations, sizes, and shapes. Some offsets exist but are typically small compared to their physical sizes.

2. Similar mass distributions between DM and baryonic components lead to a strong spin correlation between them in Lagrangian space, which is mostly conserved across the cosmic evolution. Besides, the spins of baryonic components between halos and their protohalos are also very well correlated, similar to that of the DM component. The memory of the initial perturbations of these components is not fully erased by the nonlinear structure formation.

3. Similar Lagrangian space mass distributions also enable us to use a universal spin-reconstruction algorithm for different components: similar locations, sizes, and shapes result in similar reconstructing locations, smoothing scales, and results, respectively. The spins of DM and baryonic components of total halos can be predicted by

this method in Lagrangian space. In addition, a similar result exists for central galaxies. This provides us with the possibility of using observable galaxy spins to constrain the cosmic initial conditions.

For a convergence test on resolutions, we also test the result performed on a lower resolution simulation TNG100-3. We find a good convergence between different resolution simulations with the same statistical results. Besides, various of baryonic and galaxy formation models may result in different spin correlations. We notice that some other studies using different hydrodynamic simulations all confirm DM and baryon spin correlation in Eulerian space (e.g., Teklu et al. 2015; Jiang et al. 2019). While many studies based on *N*-body simulations confirm the strong spin correlation for DM component between the Lagrangian and Eulerian spaces (e.g., Porciani et al. 2002; Wu et al. 2021), we can qualitatively infer that using different galaxy formation models will not significantly affect our statistical results. Comparing the results quantitatively based on IllustrisTNG and other hydrodynamical simulations are left to future works.

One of the main challenges of using baryonic angular momenta to reconstruct the initial conditions is to obtain the precise observational data of galaxy spin. For massive halos, various kinds of techniques are able to observe $j_{spin,CG}$, j_{orb}, or the overall angular momentum of diffuse gas in the halo (e.g., Lintott et al. 2008; Harrison et al. 2017; Graham et al. 2018). From our initial investigation, they are all reliable tracers of halo spins and primordial spin modes. Their discrepancies might contain DM–baryon segregation information (Liao et al. 2017). Another challenge is the reconstructing methods. The existing reconstructing methods, such as ELUCID, use only galaxy positions without their spins. Whether additional spin information can help improving reconstructing the initial conditions is worth studying.

On larger, more linear scales, cosmic filament spins provide more cosmological information complimentary to that of galaxies and halos (Sheng et al. 2022). It would be interesting to study the cosmic filament spins traced by baryonic matter and the spin correlations in galaxy–filament systems.

ORCID iDs

Ming-Jie Sheng ⓘ https://orcid.org/0000-0002-9891-338X

Hao-Ran Yu ⓘ https://orcid.org/0000-0001-5277-4882
Sijia Li ⓘ https://orcid.org/0000-0003-4813-8482
Shihong Liao ⓘ https://orcid.org/0000-0001-7075-6098
Min Du ⓘ https://orcid.org/0000-0001-9953-0359
Yunchong Wang ⓘ https://orcid.org/0000-0001-8913-626X
Peng Wang ⓘ https://orcid.org/0000-0003-2504-3835
Kun Xu ⓘ https://orcid.org/0000-0002-7697-3306
Shy Genel ⓘ https://orcid.org/0000-0002-3185-1540
Dimitrios Irodotou ⓘ https://orcid.org/0000-0003-2946-8080

References

Blazek, J., McQuinn, M., & Seljak, U. 2011, JCAP, 2011, 010
Catelan, P., Kamionkowski, M., & Blandford, R. D. 2001, MNRAS, 320, L7
Davis, M., Efstathiou, G., Frenk, C. S., & White, S. D. M. 1985, ApJ, 292, 371
DeFelippis, D., Genel, S., Bryan, G. L., & Fall, S. M. 2017, ApJ, 841, 16
Doroshkevich, A. G. 1970, Afz, 6, 581
Genel, S., Vogelsberger, M., Nelson, D., et al. 2013, MNRAS, 435, 1426
Graham, M. T., Cappellari, M., Li, H., et al. 2018, MNRAS, 477, 4711
Harrison, C. M., Johnson, H. L., Swinbank, A. M., et al. 2017, MNRAS, 467, 1965
Iye, M., Tadaki, K., & Fukumoto, H. 2019, ApJ, 886, 133
Jiang, F., Dekel, A., Kneller, O., et al. 2019, MNRAS, 488, 4801
Lee, J., & Libeskind, N. I. 2020, ApJ, 902, 22
Lee, J., Libeskind, N. I., & Ryu, S. 2020, ApJL, 898, L27
Lee, J., & Moon, J.-S. 2022, ApJ, 936, 119
Lee, J., & Pen, U.-L. 2000, ApJL, 532, L5
Lee, J., & Pen, U.-L. 2001, ApJ, 555, 106
Liao, S., Gao, L., Frenk, C. S., Guo, Q., & Wang, J. 2017, MNRAS, 470, 2262
Lintott, C. J., Schawinski, K., Slosar, A., et al. 2008, MNRAS, 389, 1179
Marinacci, F., Vogelsberger, M., Pakmor, R., et al. 2018, MNRAS, 480, 5113
McQuinn, M. 2021, JCAP, 2021, 024
Motloch, P., Pen, U.-L., & Yu, H.-R. 2022, PhRvD, 105, 083512
Motloch, P., Yu, H.-R., Pen, U.-L., & Xie, Y. 2021, NatAs, 5, 283
Nelson, D., Pillepich, A., Springel, V., et al. 2018, MNRAS, 475, 624
Nelson, D., Pillepich, A., Springel, V., et al. 2019a, MNRAS, 490, 3234
Nelson, D., Springel, V., Pillepich, A., et al. 2019b, ComAC, 6, 2
Peebles, P. J. E. 1969, ApJ, 155, 393
Pillepich, A., Nelson, D., Hernquist, L., et al. 2018, MNRAS, 475, 648
Pillepich, A., Nelson, D., Springel, V., et al. 2019, MNRAS, 490, 3196
Planck Collaboration, Ade, P. A. R., Aghanim, N., et al. 2016, A&A, 594, A13
Porciani, C., Dekel, A., & Hoffman, Y. 2002, MNRAS, 332, 325
Rimes, C. D., & Hamilton, A. J. S. 2005, MNRAS, 360, L82
Schmidt, F., Chisari, N. E., & Dvorkin, C. 2015, JCAP, 2015, 032
Sheng, M.-J., Li, S., Yu, H.-R., et al. 2022, PhRvD, 105, 063540
Springel, V. 2010, MNRAS, 401, 791
Springel, V., Pakmor, R., Pillepich, A., et al. 2018, MNRAS, 475, 676
Springel, V., White, S. D. M., Jenkins, A., et al. 2005, Natur, 435, 629
Springel, V., White, S. D. M., Tormen, G., & Kauffmann, G. 2001, MNRAS, 328, 726
Teklu, A. F., Remus, R.-S., Dolag, K., et al. 2015, ApJ, 812, 29
Wang, H., Mo, H. J., Yang, X., et al. 2016, ApJ, 831, 164
Wang, H., Mo, H. J., Yang, X., Jing, Y. P., & Lin, W. P. 2014, ApJ, 794, 94
Wang, P., & Kang, X. 2018, MNRAS, 473, 1562
Weinberger, R., Springel, V., & Pakmor, R. 2020, ApJS, 248, 32
White, S. D. M. 1984, ApJ, 286, 38
White, S. D. M. 1996, in Cosmology and Large Scale Structure, Proceedings of the "Les Houches Ecole d'Ete de Physique Theorique", ed. R. Schaeffer et al., Vol. 349 (Amsterdam: Elsevier), 349
Wu, Q., Yu, H.-R., Liao, S., & Du, M. 2021, PhRvD, 103, 063522
Yu, H.-R., Motloch, P., Pen, U.-L., et al. 2020, PhRvL, 124, 101302
Yu, H.-R., Pen, U.-L., & Wang, X. 2019, PhRvD, 99, 123532
Zjupa, J., & Springel, V. 2017, MNRAS, 466, 1625